

Batch norm with entropic regularization turns deterministic autoencoders into generative models

Amur Ghose and Abdullah Rashwan and Pascal Poupart

University of Waterloo, Waterloo Ontario, Canada

Vector Institute, Toronto, Ontario, Canada

{a3ghose,arashwan,ppoupart}@uwaterloo.ca

Abstract

The variational autoencoder is a well defined deep generative model that utilizes an encoder-decoder framework where an encoding neural network outputs a non-deterministic code for reconstructing an input. The encoder achieves this by sampling from a distribution for every input, instead of outputting a deterministic code per input. The great advantage of this process is that it allows the use of the network as a generative model for sampling from the data distribution beyond provided samples for training. We show in this work that utilizing batch normalization as a source for non-determinism suffices to turn deterministic autoencoders into generative models on par with variational ones, so long as we add a suitable entropic regularization to the training objective.

1 INTRODUCTION

Modeling data with neural networks is often broken into the broad classes of discrimination and generation. Generation can exist independently of tasks such as density estimation, with which it is intimately related. We consider here generation as the task of generating unseen samples from a data distribution, and specifically neural network models for the same, often simply called **deep generative models**.

The variational autoencoder (Kingma and Welling, 2013) (VAE) is a well-known subclass of deep generative models, in which we have two distinct networks - a decoder and encoder. In order to generate data with the decoder, a sampling step is introduced between the encoder and decoder. This sampling step complicates the optimization of autoencoders. Since it is not possible to differentiate through sampling steps, the reparametrization trick is of-

ten used. Furthermore, the sampling distribution must be optimized to approximate a canonical distribution such as a Gaussian. The log-likelihood objective is also approximated. Hence, it would be desirable to avoid the sampling step.

To that effect, Ghosh et al. (2019) proposed regularized autoencoders (RAEs) where the sampling step is replaced by some form of regularization since the stochasticity introduced by the sampling step can be thought as a form of regularization. By avoiding any sampling step, a deterministic autoencoder can be optimized much more simply. However, it is not clear what regularization to use and it is not clear what distribution to use to sample latent codes that could be decoded into realistic data points. Ghosh et al. (2019) fit a density to the empirical latent codes after the autoencoder has been optimized.

In this work, we propose to introduce a batch normalization step between the encoder and decoder and to add a entropic regularizer on the batch norm layer. Batchnorm fixes some moments (e.g., mean and variance) of the empirical code distribution while the entropic regularizer maximizes the entropy of the empirical code distribution. Maximizing the entropy of a distribution with certain fixed moments induces Gibbs distributions of certain families (i.e., normal distribution for fixed mean and variance). Hence, we naturally obtain a distribution that we can sample from to obtain codes that can be decoded into realistic data. The introduction of a batchnorm step with entropic regularization does not complicate the optimization of the autoencoder which remains deterministic.

The paper is organized as follows. In Section 2, we review background about variational autoencoders and batch normalization. In Section 3, we propose entropic autoencoders (EAEs) with batch normalization as a new type of deterministic generative model. Section 4 discusses the maximum entropy principle and how it naturally induces certain distributions over latent codes without any explicit entropic regularization. Section 5 demonstrates the gener-

ative performance of EAEs on three benchmark datasets (CELEBA, CIFAR-10 and MNIST). EAEs outperform previous deterministic and variational autoencoders in terms of FID scores. Section 6 concludes the paper with some suggestions for future work.

2 VARIATIONAL AUTOENCODER

The variational autoencoder (Kingma and Welling, 2013) (VAE) consists of a decoder followed by an encoder. The term autoencoder (Ng et al., 2011) is in general applied to any model that is trained to reconstruct its inputs. For a normal autoencoder, if we represent the decoder and encoder as \mathcal{D}, \mathcal{E} respectively, for every input x_i we seek to have

$$\mathcal{E}(x_i) = z_i, \mathcal{D}(z_i) = \hat{x}_i \approx x_i$$

Such a model is usually trained by minimizing $\|\hat{x}_i - x_i\|^2$ over all x_i . By contrast, in a variational autoencoder, there is no fixed codeword z_i for a x_i . Instead, we have

$$z_i = \mathcal{E}(x_i) \sim \mathcal{N}(\mathcal{E}_\mu(x_i), \mathcal{E}_{\sigma^2}(x_i))$$

That is, the encoder network calculates means and variances via $\mathcal{E}_\mu, \mathcal{E}_{\sigma^2}$ layers for every data instance, from which a code is sampled. In this instance, we devise a loss function of the form below:

$$\|\mathcal{D}(z_i) - x_i\|^2 + \beta D_{KL}(\mathcal{N}(\mathcal{E}_\mu(x_i), \mathcal{E}_{\sigma^2}(x_i)) \| \mathcal{N}(0, I))$$

where D_{KL} denotes the Kullback-Leibler divergence and z_i denotes the sample from the distribution over codes. Now, upon minimizing the above loss function over $x_i \in$ a training set, we can generate meaningful samples by a process as follows: generate $z_i \sim \mathcal{N}(0, I)$, and output $\mathcal{D}(z_i)$. The implication here is that the KL term above makes the implicitly learnt distribution of the encoder close to that of a spherical Gaussian. Usually, z_i is of a vastly smaller dimensionality than x_i .

2.1 VARIATIONS ON VARIATIONAL AUTOENCODERS

In practice, the above objective is not easy to optimize. In fact, the original VAE formulation did not involve β , and simply set it to 1. Later, it was discovered that this parameter is in fact crucial to training the VAE correctly under various scenarios, giving rise to a class of architectures termed the β -VAE. (Higgins et al., 2017)

The primary problem with the VAE lies in the training objective. Though we seek to minimize KL divergence for every instance x_i , this is often too strong. The result is a phenomenon known as **posterior collapse** (He et al., 2019) where every x_i generates $\mathcal{E}_\mu(x_i) \approx 0, \mathcal{E}_{\sigma^2}(x_i) \approx 1$. One should note that in this instance, the particular latent variable z_i begins to relate less and less to x_i , because neither μ, σ^2 depend on it. Attempts to fix this (Kim et al., 2018) involve analyzing the mutual information between z_i, x_i pairs, resulting in architectures like InfoVAE (Zhao et al., 2017). Posterior collapse is especially notable when the decoder is especially ‘powerful’, i.e. has great representational power. In practical terms, this manifests in the decoder’s depth being increased, more deconvolutional channels and so on.

One of the variations on VAEs includes creating a deterministic architecture that minimizes an optimal transport based Wasserstein loss between the latent space and the prior. Such an architecture (Tolstikhin et al., 2017) benefits from not creating a distribution for every sample. Instead, the entire posterior space is made to be close to a Gaussian distribution. This can be done by optimizing either the Maximum Mean Discrepancy (MMD) metric with a Gaussian kernel (Gretton et al., 2012), or using a GAN to minimize this optimal transport loss via Kantorovich-Rubinstein duality. In practice, the GAN variant greatly outperforms solely using MMD, causing WAE techniques to be usually considered as WAE-GAN in practice for achieving state-of-the-art results.

2.2 BATCH NORMALIZATION

Normalization is often known in statistics simply as the procedure of subtracting the mean of a dataset and dividing by the standard deviation. This identically sets the sample mean to zero and the variance to one. In neural networks, normalization on the level of a minibatch (Ioffe and Szegedy, 2015) has become ubiquitous since its introduction and is now a key part of training all forms of deep generative models (Ioffe, 2017). Given a minibatch of inputs x_i of dimensions n with μ_{ij}, σ_{ij} as its mean, standard deviation at index j respectively, we will call **BN** as the operation that satisfies:

$$[\text{BN}(x_i)]_j = \frac{x_{ij} - \mu_{ij}}{\sigma_{ij}} \quad (1)$$

Note that in practice, a batch normalization layer in a neural network computes $x_i \rightarrow A \text{BN}(x_i) + b$, i.e. an affine transform of the above. This is done during training time using the empirical average of the minibatch, and at test time using the overall averages. Many variations on this technique such as L1 normalization, instance normalization, online adaptations, etc. exist (Wu et al., 2018; Zhang

et al., 2019; Chiley et al., 2019; Ulyanov et al., 2016; Ba et al., 2016; Hoffer et al., 2018). The mechanism by which this helps optimization was initially termed as “internal covariate shift”, but later works challenge this perception (Santurkar et al., 2018; Yang et al., 2019) and it may have harmful effects (Galloway et al., 2019).

3 OUR CONTRIBUTIONS - THE ENTROPIC AUTOENCODER

Instead of outputting a distribution as VAEs do, we now seek an approach that turns deterministic autoencoders into generative models on par with VAEs. Observe that if we had a guarantee that, for a regular autoencoder that merely seeks to minimize reconstruction error, the distribution of all z_i ’s approached a spherical Gaussian, we could carry out generation just as in the VAE model. We now claim that there is a straightforward way to do this: we simply append a batch normalization step (BN as above, i.e. no affine shift) to the end of the encoder, and minimize an objective of the nature:

$$\|\hat{x}_i - x_i\|^2 - \beta H(z_i), \hat{x}_i = \mathcal{D}(z_i), z_i = \mathcal{E}(x_i) \quad (2)$$

where H represents the entropy function and is taken over a minibatch of the z_i . The key point in this approach is to notice the following. Let X be a random variable obeying $E[X] = 0, E[X^2] = 1$. Then, the maximum value of $H(X)$ is obtained iff $X \sim \mathcal{N}(0, 1)$.

3.1 EQUIVALENCE TO KL DIVERGENCE MINIMIZATION

In fact, our method of maximizing entropy is a method of minimizing the KL divergence by a backdoor. Generally, minibatches are too small to construct a meaningful sample distribution that can be compared - in D_{KL} - to the sought spherical normal distribution without other constraints. However, suppose that we have the following problem with X being a random variable with some constraint functions C_k e.g. on its moments:

$$\max H(X), E[C_k(X)] = c_k, k = 1, 2, \dots$$

In particular let the two constraints be $E[X] = 0, E[X^2] = 1$ as above. Let us have a ‘proposal’ distribution Q that satisfies $E_Q[X] = 0, E_Q[X^2] = 1$ and also a maximum entropy distribution P that is the solution to the optimization problem above. Observe that the cross entropy of P with respect to Q is

$$E_Q[-\log P(X)]$$

However, in our case, P is a Gaussian. Hence, $-\log P(X)$ solely consists of a term of the form $aX^2 + bX + c$. Upon taking expectation of this w.r.t. Q , we note that $E_Q[X], E_Q[X^2]$ are already fixed. We arrive at the fact that for all proposal distributions Q , cross entropy of P w.r.t. Q - written as $H(Q, P)$ obeys

$$H(Q, P) = H(Q) + D_{KL}(Q||P)$$

Pushing up $H(Q)$ thus directly reduces the KL divergence to P , since the left hand side is a constant. The advantage of our method relies on the fact that over a minibatch, every proposal Q identically satisfies the two moment conditions due to normalization. Unlike KL divergence, which requires estimating a conditional probability and then integrating - both of which are rapidly intractable in higher dimensions - entropy estimation is easier to handle, involves no such conditional probabilities, and forms the bedrock of estimating quantities derived from entropy such as the MI. In fact, due to interest in the Information Bottleneck method (Tishby et al., 2000) which requires entropy estimation of hidden layers in neural nets, we already have a nonparametric entropy estimator of choice - the Kozachenko Leonenko estimator (Kozachenko and Leonenko, 1987), which has the advantage of incurring very low computational load and having already been used for neural networks. Indeed, this principle of “cutting the middleman” is inspired by the fact that MI based methods for neural networks often use Kraskov-like estimators (Kraskov et al., 2004), a family of estimators that break the MI term into H terms which are estimated by the Kozachenko-Leonenko estimator. Instead of this, we directly work with the entropy.

Note that unlike MI and KL divergence based methods, our method explicitly relies on there being constraints, and that these constraints allow some sensible maximum entropy distribution that we can easily work with, such as a Gaussian. Our method thus is less general than those methods, but also far more tractable due to our usage of the entropy estimator.

3.2 A GENERIC NOTE ON THE KOZACHENKO-LEONENKO ESTIMATOR

The Kozachenko-Leonenko estimator (Kozachenko and Leonenko, 1987) operates as follows. Let $N \geq 1$ and X_1, \dots, X_{N+1} be i.i.d. samples from an unknown distribution Q . Let each $X_i \in \mathbb{R}^d$.

For each X_i , define $R_i = \min \|X_i - X_j\|_2, j \neq i$ and $Y_i = N(R_i)^d$. Let B_d be the volume of the unit ball in \mathbb{R}^d and γ the Euler-mascheroni constant ≈ 0.577 . The

Kozachenko Leonenko estimator works as follows:

$$H(Q) \approx \frac{1}{N+1} \sum_{i=1}^{N+1} \log Y_i + \log B_d + \gamma$$

Intuitively, having a high distance to the nearest training example for each example pushes up the entropy via the Y_i term. Such “repulsion”-like nearest neighbour techniques have been employed elsewhere for likelihood-free techniques such as implicit maximum likelihood estimation (Li et al., 2019; Li and Malik, 2018).

3.3 GENERALIZATION TO ANY GIBBS DISTRIBUTION

A distribution that has the maximum entropy under constraints C_k as above is called the **Gibbs distribution** of the respective constraint set. When this distribution exists, we have the result that there exists lagrange multipliers λ_k , such that if the maximum entropy distribution is P , $\log P(X)$ is of the form $\sum \lambda_k C_k$. Whenever we have any candidate distribution Q , $E_Q[C_k(X)]$ is determined solely from the constraints, and thus the cross-entropy $E_Q[-\log P(X)]$ is also determined. Therefore, our technique - of pushing up the entropy to reduce KL - holds under this generalization. As a direct result, consider $L1$ normalization layers which have been proposed as an alternative to Batch normalization. Pushing up the entropy in this case corresponds to inducing a Laplace distribution.

3.4 PARALLELS WITH THE CONSTANT VARIANCE VAE

One of the variations on VAEs include the constant variance VAE (Ghosh et al., 2019), where the term \mathcal{E}_{σ^2} is a constant for every instance x_i . Under such a case, let us consider transmitting a code via the encoder that maximizes $MI(X, Y)$ where X is the encoder’s output and Y the input to the decoder.

Observe that for a discrete-valued random variable X , $MI(X, X) = H(X)$. That is, if noiseless transmission was possible, the mutual information would depend solely on the entropy. We are, however, using continuous random variables. Our analysis of the constant variance autoencoder would for $\sigma^2 = 0$ yield a MI of ∞ , between the code emitted by the encoder and received by the decoder. This, at first glance, appears ill-defined.

However, suppose that we are in the test conditions i.e. the batch normalization is using a fixed mean and variance and not dependent on the minibatch. Under this case, if the decoder receives Y , $MI(X, Y) = H(X) - H(X|Y)$. Since $(X|Y)$ is a Dirac distribution, it pushes the mutual

information to ∞ . However, if we ignore the infinite mutual information introduced by the deterministic mapping just as we do in the definition of differential entropy, the only term remaining is $H(X)$, maximizing which becomes equivalent to maximizing MI.

Consequently, we posit that our model can be seen as the zero-variance limit of present constant variance VAE architectures, especially in situations where the batch size is large enough to allow accurate estimations of mean and variance.

3.5 COMPARISON TO PRIOR DETERMINISTIC AUTOENCODERS

Our work is not the first to use a deterministic autoencoder as a generative one. However, prior attempts in this regard such as regularized autoencoders (RAEs) (Ghosh et al., 2019) are completely different, and do not leverage batch normalization. Rather, these methods rely on taking the constant variance autoencoder, and imposing a regularization term on the architecture. This does not maintain the KL property that we show arises via entropy maximization, rather, it forms a latent space that has to be estimated such as via a Gaussian mixture model (GMM) on top of the regularization. The Gaussian latent space is thus lost, and has to be estimated post-training. This does not occur in our model. Compared to the prior Wasserstein autoencoder (WAE) (Tolstikhin et al., 2017), RAEs achieve better empirical results, however we further improve on these results while keeping the ability to sample from the prior i.e. isotropic Gaussians. As such, we combine the ability of WAE-like sampling with performance superior to RAEs, delivering the best of both worlds.

4 THE MAXIMUM ENTROPY PRINCIPLE AND REGULARIZER-FREE LATENTS

We now turn to a general framework that motivates our architecture and adds context. Given the possibility of choosing a distribution $Q \in \mathcal{D}$ that fits some given dataset \mathcal{X} provided, what objective should we choose? One choice is to pick:

$$Q = \arg \max_{Q \in \mathcal{D}} E_{\mathcal{X}}[LL_Q(X)]$$

where $LL_Q(X)$ denotes the log likelihood of an instance X and $E_{\mathcal{X}}$ indicates that the expectation is taken with the empirical distribution $\bar{\mathcal{X}}$ from \mathcal{X} , i.e. every point X is assigned a probability $\frac{1}{|\mathcal{X}|}$. An alternative is to pick:

$$Q = \arg \max_{Q \in \mathcal{D}} H(Q) \quad (3)$$

$$\text{subject to } T_i(Q) = T_i(\mathcal{X}) \quad (4)$$

Where H is the entropy of Q , and $T_i(Q)$ are summary statistics of Q that match the summary statistics over the dataset. For instance, if all we know is the mean and variance of \mathcal{X} , the distribution Q with maximum entropy that has the same mean and variance is Gaussian. This so-called maximum entropy principle (Bashkirov, 2004) has been used in various forms in reinforcement learning (Ziebart et al., 2008), natural language processing (Berger et al., 1996) and computer vision (Skilling and Bryan, 1984) successfully.

4.1 THE MAXENT PRINCIPLE APPLIED TO DETERMINISTIC AUTOENCODERS

Now, consider the propagation of an input through an autoencoder. The autoencoder may be represented as:

$$X \approx \mathcal{D}(\mathcal{E}(X))$$

where \mathcal{D}, \mathcal{E} respectively represent the decoder and encoder halves. Now, observe that if we add a BatchNorm of the form $A \circ B$ with A as an affine shift and B as **BN** (as defined in Equation 1) to \mathcal{E} - the encoder - we are effectively asking to find a distribution Z after B and before A , such that:

- $E[Z] = 0, E[Z^2] = 1$
- $B \circ \mathcal{E}(X) \sim Z, A \circ \mathcal{D}(Z) \sim X$

Observe that there are two conditions which do not depend on \mathcal{E}, \mathcal{D} : $E[Z] = 0, E[Z^2] = 1$. Consider two different optimization problems:

- O , which asks to find the max entropy distribution Q , i.e., with $\max H(Q)$ over Z satisfying $E_Q[Z] = 0, E_Q[Z^2] = 1$.
- O' , which asks to find $\mathcal{D}, \mathcal{E}, A$ and a distribution Q' over Z such that we maximize $H(Q')$, with $E_{Q'}[Z] = 0, E_{Q'}[Z^2] = 1, B \circ \mathcal{E}(X) \sim Z, A \circ \mathcal{D}(Z) \sim X, Z \sim Q'$.

Since O has fewer constraints, $H(Q) \geq H(Q')$. Furthermore, $H(Q)$ is known to be maximal iff Q is an isotropic Gaussian over Z . However, what happens as the capacity of \mathcal{D}, \mathcal{E} rise to the point of possibly representing anything (e.g., by increasing depth)? The constraints

$B \circ \mathcal{E}(X) \sim Z, A \circ \mathcal{D}(Z) \sim X, Z \sim Q'$ effectively vanish. We can take the solution of O , plug it into O' , and find $\mathcal{E}, \mathcal{D}, A$ that (almost) meet the constraints of $B \circ \mathcal{E}(X) \sim Z, A \circ \mathcal{D}(Z) \sim X, Z \sim Q'$. Therefore, if the algorithm chooses the max entropy solution, the solution of O' - the actual distribution after the BatchNorm layer - approaches the maxent distribution, an isotropic Gaussian, when the last three constraints in O affect the solution less.

4.2 NATURAL EMERGENCE OF GAUSSIAN LATENTS IN DEEP NARROWLY BOTTLENECKED AUTOENCODERS

We make interesting prediction: if we increase the depths of \mathcal{E}, \mathcal{D} and constrain \mathcal{E} to output a code Z obeying $E[Z] = 0, E[Z^2] = 1$, the distribution of Z should - even without an entropic regularizer - tend to go to a spherical Gaussian as depth increases relative to the bottleneck. In practical terms, this will manifest in less regularization being required at higher depths or narrower bottlenecks for our model. Note that this phenomenon also occurs in posterior collapse for VAEs, hence, we should verify that our latent space stays meaningful under such conditions.

Under the information bottleneck principle, for a neural network with output Y from input X , we seek a hidden layer representation for Z that maximizes $\text{MI}(Z, Y)$ while lowering $\text{MI}(X, Z)$. For an autoencoder, $Y \approx X$. As such, since Z is fully determined from X in a deterministic autoencoder, increasing $H(Z)$ increases $\text{MI}(Z, X)$ if we ignore the ∞ term that arises due to $H(Y|X)$ as Y approaches a deterministic function of X as before in our discussion of CV-VAEs. As such, increasing $H(Z)$ will be justified iff it gives rise to better reconstruction, i.e. making Z more entropic (informative) lowers the reconstruction loss.

Such an increase is likelier when Z is of low dimensionality, and struggles to summarize X . We come to a concrete prediction: a deep, and narrowly bottlenecked autoencoder with a batch normalized code, will, even in the absence of regularization, approach spherical Gaussian-like latent spaces. We show this to be true in the datasets of interest, where narrow enough bottlenecks can yield samples even **without** regularization, a behaviour also anticipated in (Ghosh et al., 2019).

5 EMPIRICAL EXPERIMENTS

5.1 BASELINE ARCHITECTURES WITH ENTROPIC REGULARIZATION

We begin by generating images based on our architecture on 3 standard datasets, namely MNIST (LeCun et al.,

2010), CIFAR-10 (Krizhevsky et al., 2014) and CelebA (Liu et al., 2018). Specifically, we use convolutional channels of [128, 256, 512, 1024] in the encoder half and deconvolutional channels of [512, 256] for MNIST and CIFAR-10 and [512, 256, 128] for CelebA, starting from an initial channel size of 1024 in the decoder half. For kernels we use 4×4 for CIFAR-10 and MNIST, and 5×5 for CelebA with strides of 2 for all layers except the terminal layer in the decoder. Each layer utilizes a subsequent batchnorm layer along with ReLU activations, and the hidden bottleneck layer immediately after the encoder has a batch norm sans affine shift as discussed above. These architectural details, preprocessing of datasets, etc. match exactly the previous architectures that we benchmark against (Ghosh et al., 2019; Tolstikhin et al., 2017).

For optimization, we utilize the ADAM optimizer. The minibatch size is set to 100 with an entropic regularization based on the Kozachenko Leonenko estimator (Kozachenko and Leonenko, 1987). In terms of latent dimensionality, we use 16 for MNIST, 128 for CIFAR-10 and 64 for CelebA. At most 100 epochs are used for MNIST and CIFAR-10 and at most 70 for CelebA.

In Figure 1, we present qualitative results on the MNIST dataset. Note that we do not report the Frechet Inception Distance (FID) (Heusel et al., 2017), a commonly used metric for gauging image quality, since it uses the Inception network, which is not calibrated on grayscale handwritten digits. In figure 1, we show the the quality of the generated images for two different regularization weights β in Eq. 2 (0.0516 and 1.032 respectively) and in the same figure illustrate the quality of reconstructed digits.

We now move on to qualitative results for CelebA. We present a collage of generated samples in Figure 2. CIFAR-10 samples are presented in Figure 3. We also seek to compare, thoroughly, to the RAE architecture. For this, we present quantitative results in terms of FID scores in Table 1. We show results when sampling latent codes from an isotropic Gaussian as well as from densities fitted to the empirical distribution of latent codes after the AE has been optimized. As done in previous work, we consider densities that consist of multivariate Gaussians (MVGs) with full covariance and Gaussian mixture models (GMMs). In all cases, we improve on RAE-variant architectures proposed previously (Ghosh et al., 2019). We refer to our architecture as the **entropic autoencoder (EAE)**.

DETAILS ON PREVIOUS TECHNIQUES

In the consequent tables and figures, VAE/AE have their standard meanings. AE-L2 refers to an autoencoder with

only reconstruction loss and L2 regularization, 2SVAE to the Two-Stage VAE as per (Dai and Wipf, 2019), WAE to the Wasserstein Autoencoder as per (Tolstikhin et al., 2017), RAE to the Regularized Auto-encoder as per (Ghosh et al., 2019), with RAE-L2 referring to such with a L2 penalty, RAE-GP to such with a Gradient Penalty, RAE-SN to such with spectral normalization. We use spectral normalization in our EAE models for CelebA, and L2 regularization for CIFAR-10.

QUALITATIVE COMPARISON TO PREVIOUS TECHNIQUES

While Table 1 captures the quantitative performance of our method, we seek to provide a qualitative comparison as well. This is done in Figure 4. We compare to all RAE variants, as well as 2SVAE, WAE, CV-VAE and the standard VAE and AE as in Table 1. Results for CIFAR-10 and MNIST appear in the supplementary material.

5.2 GAUSSIAN LATENTS WITHOUT ENTROPIC REGULARIZATION

A somewhat surprising result emerges as we make the latent space dimensionality lower while ensuring a complex enough decoder and encoder. Note that even though earlier we discussed this process in the context of depth, our architectures are convolutional and a better heuristic proxy is the number of channels while keeping the depth constant. To that end, we note that all our encoders share a power of 2 framework, i.e. channels double every layer from 128. Keeping this doubling structure, we ask ourselves what is the effect of width on the latent space when the entropic regularizer does not exist. We set the channels to double from 64, i.e. 64, 128, 256, 512 and correspondingly in the decoder for MNIST. Figure 5 shows the samples with the latent dimension being set to 8, and also the result when we take corresponding samples from an isotropic Gaussian when the number of latents is instead 32.

There is a large drop in sample quality, as is visually evident, by going from a narrow autoencoder to a wide one for the purposes of generation, when no constraints on the latent space are employed. To confirm the analysis, we provide the result for 16 dimensions in the figure as well, which is intermediate in quality between the two extremes.

The aforesaid effect is not restricted to MNIST. We perform a similar study on CelebA taking the latent space from 48 to 128, and the results in Figures 6 and 7 show a corresponding change in sample quality. Of course, the results with 48 dimensional unregularized latents are worse than our regularized, 64 dimensional sample collage in



Figure 1: Left: Generated MNIST images with $\beta = 0.0516$ in Eq. 2. Middle: Generated MNIST images with $\beta = 1.032$ in Eq. 2. Right: Reconstructed MNIST images with $\beta = 1.032$ in Eq. 2.

Architecture	CIFAR-10-Iso	CelebA-Iso	CIFAR-10-MVG	CelebA-MVG	CIFAR-10-GMM	CelebA-GMM
VAE	106.37	48.12	N/A	N/A	103.78	45.52
CV-VAE	94.75	48.87	N/A	N/A	86.64	49.30
WAE	117.44	53.67	N/A	N/A	93.53	42.73
2SVAE	109.77	49.70	N/A	N/A	N/A	N/A
RAE	N/A	N/A	83.87	48.20	76.28	44.68
RAE-L2	N/A	N/A	80.80	51.13	74.16	47.97
RAE-GP	N/A	N/A	83.05	116.30	76.33	45.63
RAE-SN	N/A	N/A	84.25	44.74	75.30	40.95
AE	N/A	N/A	84.74	127.85	76.47	45.10
AE-L2	N/A	N/A	247.48	346.29	75.40	48.42
EAE	85.26(84.53)	44.63	80.07	42.92	73.12	39.76

Table 1: FID scores for relevant VAEs and VAE-like architectures. Scores within parentheses for EAE denote a regularization on a linear map. Iso denotes samples drawn from a latent space of $\mathcal{N}(0, I)$, while MVG denotes sampling from a post-training density estimation step done via creating a Multivariate Gaussian with full covariance, i.e. from $\mathcal{N}(\mu, \Sigma)$. GMM denotes sampling from a mixture of 10 such Gaussians, fit similarly. These evaluations correspond to analogous benchmarking for RAEs. (Ghosh et al., 2019)

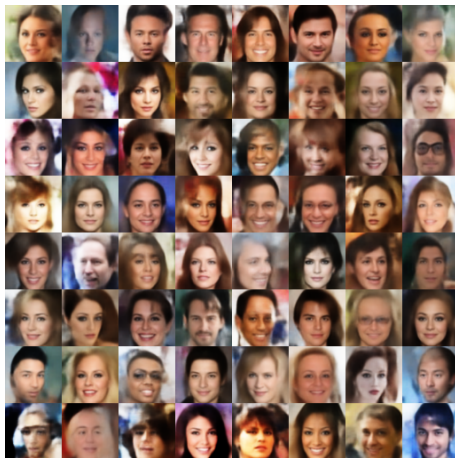


Figure 2: Generated images on CelebA

Figure 2, but they retain facial quality without artifacts. The FID scores (provided in caption) also follow this trend.

Recall that in our formulation of the MaxEnt principle, we considered more complex maps (e.g., deeper or wider networks with possibly more channels) able to induce more arbitrary deformations between a latent space and the target space. A narrower bottleneck incentivizes Gaus-

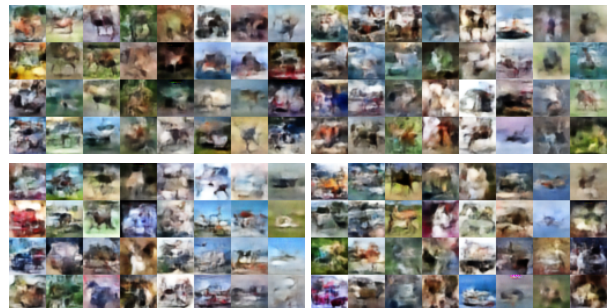


Figure 3: Generated images on CIFAR-10, under four different regularization weights (top left $\beta = 0.505$, top right $\beta = 0.707$, bottom left $\beta = 0.0505$, bottom right $\beta = 0.0707$).

sianization - with a stronger bottleneck, there is more incentive to make sure each latent carries more information, incentivizing higher entropy in codes Z , as discussed in our parallels with Information Bottleneck-like methods.

We present a similar analysis between CIFAR-10 AEs without regularization. Unlike the previous case, CIFAR-10 samples suffer from the issue that visual quality is not all that evident to the human eye. These figures are presented in Figures 8 and 9. The approximate FID difference between these two images is roughly 13 points (≈ 100 vs ≈ 87). While FID scores are not all that

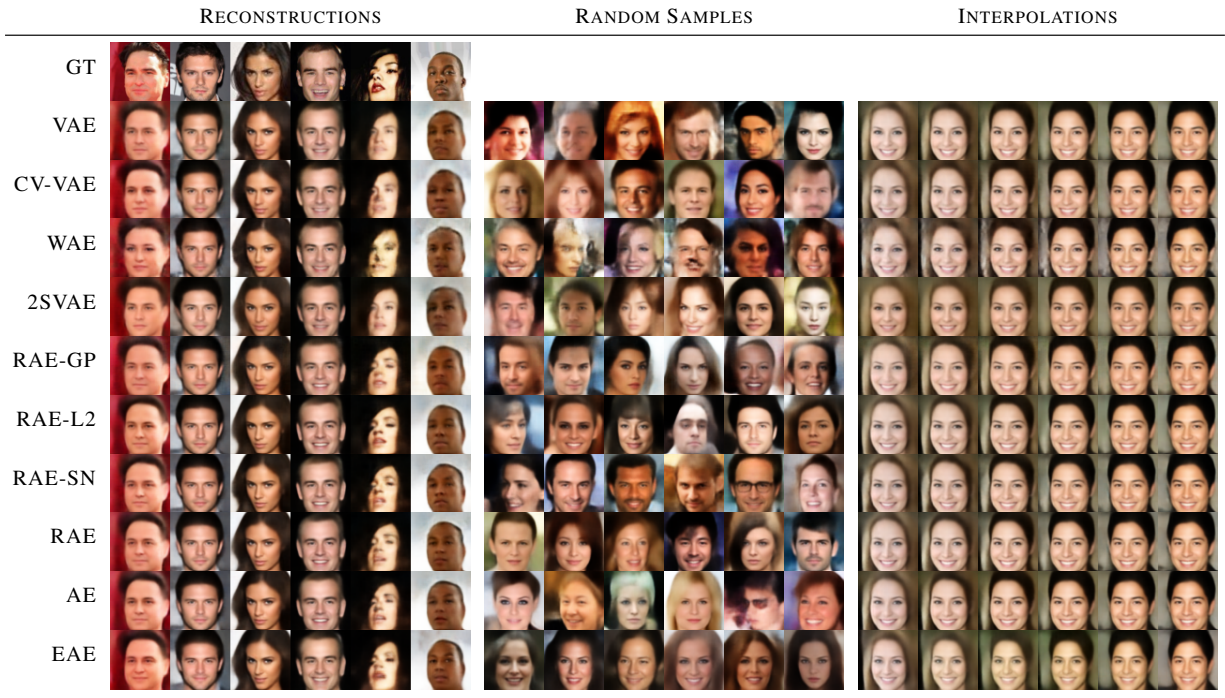


Figure 4: Qualitative comparisons to RAE variants and other standard benchmarks on CelebA. On the left, we have reconstructions (top row being ground truth GT), the middle has generated samples, the right has interpolations. From top to bottom ignoring GT: VAE, CV-VAE, WAE, 2SVAE, RAE-GP, RAE-L2, RAE-SN, RAE, AE, EAE. Non-EAE figures reproduced from (Ghosh et al., 2019)



Figure 5: Variation in bottleneck width causes massive differences in generative quality sans regularization. From left to right, we present samples (from $\mathcal{N}(0, I)$ for 8, 16, 32 dimensional latent spaces)

meaningful for MNIST, we can compare CelebA and CIFAR-10 in terms of FID scores (provided in figure captions). These back up our assertions. Note that for all comparisons, only the latent space is changed and the best checkpoint is taken for both models, hence we have a case of a strictly less complex model outperforming another that does not arise due to more channels allowing for a better reconstruction, explainable in MaxEnt terms.

6 CONCLUSIONS AND FUTURE WORK

The VAE has long remained one of the most popular deep generative models. At the same time, it has drawn criticism for its blurry images, posterior collapse and other issues. Deterministic encoders have been posited as

an escape from blurriness, since they ‘lock’ codes into a single choice for each instance. In this regard, we consider our work as reinforcing Wasserstein autoencoders and other recent work in deterministic autoencoders such as RAEs (Ghosh et al., 2019). In particular, we consider our method of raising entropy to be generalizable whenever batch normalization is in play, and we note that it solves a considerably more specific problem than reducing the KL between two arbitrary distributions P, Q to one where both P, Q satisfy moment constraints. Such reductions can - as in this instance - make difficult problems tractable via simple estimators.

In our experiments, we initially hoped to obtain results via sampling from a prior distribution that were, without ex-post density estimation, already state of the art. In practice, we observed that using a GMM to fit the density



Figure 6: Generated images on CelebA with a narrow bottleneck of 48, unregularized. The associated FID score was 53.82.



Figure 7: Generated images on CelebA with latent dimensions of 128, also unregularized. This associates a FID score of 64.72.

greatly improves results, regardless of architecture. These findings might be explained in light of the 2-stage VAE analysis (Dai and Wipf, 2019), wherein it is postulated single-stage VAEs inherently struggle to capture gaussian latents, and a second stage is amenable. To this end, we might aim to design a 2-stage EAE. Numerically, we found such an architecture hard to tune, as opposed to a single stage EAE which was remarkably robust to the choice of hyperparameters. As such, we believe this might be an interesting future direction.

Finally, we note that our results improve on the RAE, which in turn improved on the 2SVAE FID numbers. Though the latest and greatest GAN architectures remain out of reach in terms of FID scores for most VAE models, 2SVAE came within striking distance of somewhat older ones, such as the vanilla WGAN. Integrating state of the art techniques for VAEs as in, for instance, VQVAE2 (Razavi et al., 2019) to challenge GAN-level benchmarks could form an interesting future direction. Quantized latent spaces also offer a much more tractable framework for entropy based models and allow us to work with discrete entropy which is a more meaningful function.

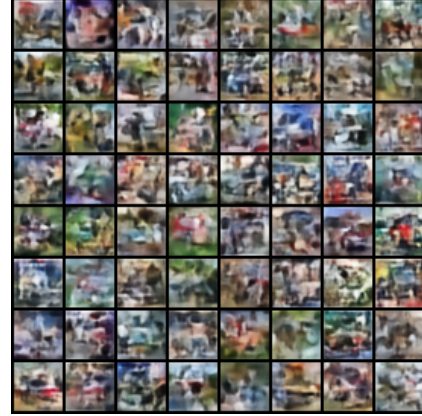


Figure 8: Generated images on CIFAR-10 with unregularized latent dimension of 128. The FID score is 100.62, with L2 regularization.

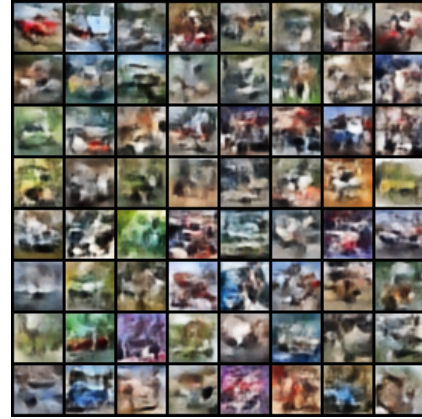


Figure 9: Generated images on CIFAR-10 with unregularized latent dimension equal to 64. The FID score associated with this checkpoint is 87.45, trained using L2 regularization.

The previous work on RAEs (Ghosh et al., 2019), which our method directly draws on deserves special addressal. The RAE method shows that deterministic autoencoders can succeed at generation, so long as regularizers are applied and post-density estimation is carried out. Yet, while regularization is certainly nothing out of the ordinary, the density estimation step robs RAEs of sampling from any isotropic prior or indeed any prior for that matter. We improve on the RAE techniques when density estimation is in play, but more pertinently, we keep a method for isotropic sampling that is rigorously equivalent to cross entropy minimization. As such, we offer better performance while adding more features, and our isotropic results far outperform comparable isotropic benchmarks.

References

J L Ba, J R Kiros, and G E Hinton. Layer normalization. *arXiv:1607.06450*, 2016.

- AG Bashkurov. On maximum entropy principle, superstatistics, power-law distribution and renyi parameter. *Physica A: Statistical Mechanics and its Applications*, 340(1-3):153–162, 2004.
- A L Berger, V J D Pietra, and S A D Pietra. A maximum entropy approach to natural language processing. *Computational linguistics*, 22(1):39–71, 1996.
- V Chiley, I Sharapov, A Kosson, U Koster, R Reece, S S de la Fuente, V Subbiah, and M James. Online normalization for training neural networks. *arXiv:1905.05894*, 2019.
- B Dai and D Wipf. Diagnosing and enhancing vae models. *arXiv:1903.05789*, 2019.
- A Galloway, A Golubeva, T Tanay, M Moussa, and G W Taylor. Batch normalization is a cause of adversarial vulnerability. *arXiv:1905.02161*, 2019.
- P Ghosh, M SM Sajjadi, A Vergari, M Black, and B Schölkopf. From variational to deterministic autoencoders. *arXiv:1903.12436*, 2019.
- A Gretton, K M Borgwardt, M J Rasch, B Schölkopf, and A Smola. A kernel two-sample test. *JMLR*, 13(Mar): 723–773, 2012.
- J He, D Spokoyny, G Neubig, and T Berg-Kirkpatrick. Lagging inference networks and posterior collapse in variational autoencoders. *arXiv:1901.05534*, 2019.
- M Heusel, H Ramsauer, T Unterthiner, B Nessler, and S Hochreiter. Gans trained by a two time-scale update rule converge to a local nash equilibrium. In *NeurIPS*, pages 6626–6637, 2017.
- I Higgins, L Matthey, A Pal, C Burgess, X Glorot, M Botvinick, S Mohamed, and A Lerchner. beta-vae: Learning basic visual concepts with a constrained variational framework. *ICLR*, 2(5):6, 2017.
- E Hoffer, R Banner, I Golan, and D Soudry. Norm matters: efficient and accurate normalization schemes in deep networks. In *NeurIPS*, pages 2160–2170, 2018.
- S Ioffe. Batch renormalization: Towards reducing mini-batch dependence in batch-normalized models. In *NeurIPS*, pages 1945–1953, 2017.
- S Ioffe and C Szegedy. Batch normalization: Accelerating deep network training by reducing internal covariate shift. *arXiv:1502.03167*, 2015.
- Y Kim, S Wiseman, A C Miller, D Sontag, and A M Rush. Semi-amortized variational autoencoders. *arXiv:1802.02550*, 2018.
- D P Kingma and M Welling. Auto-encoding variational bayes. *arXiv:1312.6114*, 2013.
- LF Kozachenko and Nikolai N Leonenko. Sample estimate of the entropy of a random vector. *Problemy Peredachi Informatsii*, 23(2):9–16, 1987.
- A Kraskov, H Stögbauer, and P Grassberger. Estimating mutual information. *Physical review E*, 69(6):066138, 2004.
- A Krizhevsky, V Nair, and G Hinton. The cifar-10 dataset. online: <http://www.cs.toronto.edu/kriz/cifar.html>, 55, 2014.
- Y LeCun, C Cortes, and CJ Burges. Mnist handwritten digit database. *AT&T Labs [Online]*. Available: <http://yann.lecun.com/exdb/mnist>, 2:18, 2010.
- K Li and J Malik. Implicit maximum likelihood estimation. *arXiv preprint arXiv:1809.09087*, 2018.
- K Li, T Zhang, and J Malik. Diverse image synthesis from semantic layouts via conditional imle. In *ICCV*, pages 4220–4229, 2019.
- Z Liu, P Luo, Xiaogang Wang, and Xiaoou Tang. Large-scale celebfaces attributes (celeba) dataset. *Retrieved August*, 15:2018, 2018.
- Andrew Ng et al. Sparse autoencoder. *CS294A Lecture notes*, 72(2011):1–19, 2011.
- A Razavi, A van den Oord, and O Vinyals. Generating diverse high-fidelity images with vq-vae-2. In *NeurIPS*, pages 14837–14847, 2019.
- S Santurkar, D Tsipras, A Ilyas, and A Madry. How does batch normalization help optimization? In *NeurIPS*, pages 2483–2493, 2018.
- J Skilling and RK Bryan. Maximum entropy image reconstruction-general algorithm. *Monthly notices of the royal astronomical society*, 211:111, 1984.
- N Tishby, F C Pereira, and W Bialek. The information bottleneck method. *arXiv*, 2000.
- I Tolstikhin, O Bousquet, S Gelly, and B Schoelkopf. Wasserstein auto-encoders. *arXiv:1711.01558*, 2017.
- D Ulyanov, A Vedaldi, and V Lempitsky. Instance normalization: The missing ingredient for fast stylization. *arXiv:1607.08022*, 2016.
- S Wu, G Li, L Deng, L Liu, D Wu, Y Xie, and L Shi. L1-norm batch normalization for efficient training of deep neural networks. *IEEE transactions on neural networks and learning systems*, 2018.
- G Yang, J Pennington, V Rao, J Sohl-Dickstein, and S S Schoenholz. A mean field theory of batch normalization. *arXiv:1902.08129*, 2019.
- H Zhang, Y N Dauphin, and T Ma. Fixup initialization: Residual learning without normalization. *arXiv:1901.09321*, 2019.
- S Zhao, J Song, and S Ermon. Infovae: Information maximizing variational autoencoders. *arXiv:1706.02262*, 2017.

B D Ziebart, A Maas, J A Bagnell, and A K Dey. Maximum entropy inverse reinforcement learning. 2008.

SUPPLEMENTARY MATERIAL

On the next two pages, we present additional qualitative results.



Figure 10: Qualitative comparisons to RAE variants and other standard benchmarks on CIFAR-10. On the left, we have reconstructions (top row being ground truth GT), the middle has generated samples, the right has interpolations. From top to bottom ignoring GT: VAE, CV-VAE, WAE, 2SVAE, RAE-GP, RAE-L2, RAE-SN, RAE, AE, EAE. Non-EAE figures reproduced from (Ghosh et al., 2019)

	RECONSTRUCTIONS	RANDOM SAMPLES	INTERPOLATIONS
GT	4 1 7 5 3 6		
VAE	4 1 7 5 3 6	3 5 4 2 8 7	2 2 2 6 6 6
CV-VAE	4 1 7 5 3 6	3 7 8 3 9 2	2 2 2 6 6 6
WAE	4 1 7 5 3 6	0 6 5 1 3 2	2 2 2 6 6 6
2SVAE	4 1 7 5 3 6	9 1 9 5 2 6	2 2 2 6 6 6
RAE-GP	4 1 7 5 3 6	3 6 3 3 0 0	2 2 2 6 6 6
RAE-L2	4 1 7 5 3 6	6 4 6 6 0 0	2 2 2 6 6 6
RAE-SN	4 1 7 5 3 6	1 8 1 0 1 3	2 2 2 6 6 6
RAE	4 1 7 5 3 6	5 7 8 8 4 9	2 2 2 6 6 6
AE	4 1 7 5 3 6	2 0 7 2 1 7	2 2 2 6 6 6
EAE	4 1 7 5 3 6	0 2 9 1 9 5	2 2 2 6 6 6

Figure 11: Qualitative comparisons to RAE variants and other standard benchmarks on MNIST. On the left, we have reconstructions (top row being ground truth GT) , the middle has generated samples, the right has interpolations. From top to bottom ignoring GT: VAE, CV-VAE, WAE, 2SVAE, RAE-GP, RAE-L2, RAE-SN, RAE, AE, EAE. Non-EAE figures reproduced from (Ghosh et al., 2019)